Piezoelectric Material Tailoring for Vibrations Energy Harvesters Power Optimization

A.M. Matos∗[1], J.M. Guedes∗[2], K.P. Jayachandran, H.C. Rodrigues

IDMEC, IST, Department of Mechanical Engineering, Technical University of Lisbon, Av. Rovisco Pais, 1049-001 Lisbon, Portugal

∗[1]ago.matoz@gmail.com ; ∗[2]jmguedes@tecnico.ulisboa.pt

October, 2014

Abstract: This work presents piezoelectric material tailoring by the method of asymptotic homogenization to create piezoelectric vibrations energy harvesters capable of producing higher electrical power. The considered piezoelectric materials are $BaTiO_3$ and PZN-4.5%PT single crystals. A computational model is developed to optimize the harvester output power considering the unimorph traditional vibration harvester configuration. The unimorph is tuned for ambient vibrations and modelled using the finite element method. Single crystal, polycrystalline materials and piezocomposites made by piezoelectric and polymer materials are considered in the optimization procedures. Polycrystalline and piezocomposites properties are computed through a computational model based in the homogenization theory and implemented using the finite element method. As design variables one considers, for the single crystal case its orientation, for the polycrystalline material the microstructural orientation distribution of the grains and for the piezocomposite the piezoelectric material orientation or grains orientations in the case of polycrystalline, the unit cell piezoelectric material volume fraction and polymer orientation. A simulated annealing algorithm is used as optimizer. Several examples are presented and discussed considering excitation near and far away of resonance frequency for unimorph configuration. Also sensitivity for the electric circuit resistance is performed.

1. Introduction

The recent advancements in materials & circuits technologies plus low power consumption devices encourage the use of piezoelectric materials for vibrations energy harvesting [1 to 2]. These harvesters use the piezoelectric effect to convert directly mechanical vibrations into electrical energy with a circuit help connected to electrodes. In this paper it is considered the harvester configuration unimorph, subjected to different loadings. The harvester can be modelled using the finite element (FE) method since previous works using this method have shown good approximation to the experimental results [3 to 6]. In the work [7] the referred four configurations were studied in detail for harvesting purposes using the FE method. The present study uses some optimum orientations of [7] and the objective is to achieve higher power output by tailoring piezoelectric material properties. Piezoelectric materials properties can be tailored building a composite macrostructure [8 to 9] of piezoelectric rods and a polymer matrix for example, doping piezoelectric material [10 to 12] or creating a composite microstructure [13 to 15] which can involve topology optimization, crystals orientation optimization, etc. The material tailoring method chosen in this work is the method of asymptotic homogenization (MAH) which allows calculating the effective/macro properties of a material made by a generic periodic microstructure. These macro/effective properties can be calculated building a microstructure using the FE method [13 to 16] which is periodic. In [17] it is compared the Young modulus of bone tissue between experimental and numerically homogenized bone tissue (using FE method for microstructure and MAH) obtaining near results for some cases showing the chosen method as one capable of reproducing experimental results.

A group of piezoelectric materials typically used for energy harvesting are the piezoelectric ceramics [1 to 2]. Among these materials lead zirconate titanate (PZT) and barium titanate ($BaTiO_3$) exhibit very high dielectric and piezoelectric properties being suitable for piezoelectric energy harvesters [1 to 2 & 7]. The piezoelectric ceramics are crystalline solids with a single crystal or polycrystalline microstructure. The polycrystalline solid grains or crystals orientations plus shape and grain boundaries can be known using X-ray diffraction contrast tomography [18 to 19]. In this work it is assumed the crystals orientations distribution in a polycrystalline piezoelectric ceramic material is a Gaussian or normal distribution as in [14]. The conventional methods to characterize the polycrystalline piezoelectric ceramics properties can be found in [20]. Previous works [21] have shown the value of piezoelectric and dielectric constants change with grain size for $BaTiO_3$ showing the piezoelectric material properties can change with average grain or crystal size variation. The reason for this effect is not clearly understood. Each grain or crystal properties can be characterized using [22, 23] methods. In [24] Shu et al. studied the grain boundaries effects on piezoelectric and dielectric properties of PZT ($PbTiO_3$) simulating polycrystalline ferroelectrics polarization evolution using the finite element method, founding significant variations of properties with the grain boundary thickness. In the present work the grain boundary and grain size contributions to piezoelectric properties are ignored. This is important since in this work the MAH will be applied considering the periodic microstructure made of piezoceramic crystals or a composite of piezoceramic crystals and a polymer. This polymer can be also piezoelectric [25]. The piezopolymers have lower piezoelectric coupling properties than piezoceramics but have a significantly bigger flexibility. This allows thinking creating a composite piezoelectric material with high piezoelectric constants and good flexibility being suitable for low wind speed energy harvesters [26], automobile tire harvesters [27], etc.

This work is divided in X parts. In the first part it is presented the piezoceramics single crystal properties, the obtained homogenization equations & related finite element mesh, the optimization procedure and the considered harvesters configurations. In the second part it is calculated the partial derivatives for the harvested power. Based in these results it is identified some polymers which could increase power. Finally in the third part it is shown that the harvested power can be increased by choosing appropriate polymers.

2. Material Properties, Homogenization & Related Finite Element Mesh

In this section the material properties for barium titanate (BaTio3) and lead zirconate niobate-lead titanate (PZN-4.5%PT) single crystals are presented. Next the method of asymptotic homogenization is applied and resulted equations for macroscopic properties are presented. The finite element mesh for which the equations will be solved and the available options to build a composite material or piezopolymer with a piezoceramic and a polymer are presented.

2.1. Single Crystals, Polymer & Substrate Materials Properties

The single crystals properties are presented in tables 1 to 4 for barium titanate BaTio3, lead zirconate niobate-lead titanate PZN-4.5%PT and polyvinyledenedifluoride–trifluoroethylene PVDF-TrFE. The presented values are taken from [22,23,28]. Properties are in the IEEE format, i.e., the order used for the material matrices is [1,2,3,23,13,12]. The crystals and polymer are transversely isotropic. PZN-4.5%PT is poled along z-direction. The BaTio3, PZN-4.5%PT and PVDF-TrFE densities are 6020, 8310 and 1770 Kg/m^3 respectively.

S^E in $\times\ 10^{-12}\ (m^2/N)$	S^E_{11}	S^E_{12}	S^E_{13}	S^E_{33}	S^E_{44}	S^E_{66}
PZN-4.5%PT	82	-28.5	-51	108	15.6	15.9
$BaTiO_3$	7.38	-1.39	-4.41	13.1	16.4	7.46

Table 1 – Piezoelectric materials compliance properties

S^E in $\times\ 10^{-10}\ (m^2/N)$	S^E_{11}	S^E_{12}	S^E_{13}	S^E_{33}	S^E_{44}	S^E_{66}
PVDF-TrFE	3.28	-1.44	-0.88	3.01	190	9.43

Table 2 – Polymer material compliance matrix

d in $\times\ 10^{-12}\ (C/N)$	d_{31}	d_{33}	d_{15}
PZN-4.5%PT	-970	2000	140
$BaTiO_3$	-33.72	93.95	560.7
PVDF-TrFE	10.5	-33.81	-38.0

Table 3 – Piezoelectric materials coupling matrix properties

ε^T in $\times\ 8.85\times\ 10^{-12}\ (F/m)$	ε_{11}	ε_{33}
PZN-4.5%PT	3100	5200
$BaTiO_3$	2200	56
PVDF-TrFE	7.51	8.0

Table 4 – Piezoelectric materials dielectric coefficients

The different single crystals and PVDF-TrFE mechanical quality factors are presented in table 5 [29 to 31].

Material	*Q*
PZN-4.5%PT	139
$BaTiO_3$	1300
PVDF-TrFE	40

Table 5 – Mechanical quality factor

In unimorph harvester configurations it is needed a substrate material. In this work the considered substrate is brass. The brass mechanical properties are [32,33] a 97 (GPa) Young modulus, density 8490 (Kg/m^3), Poisson ratio 0.31 and a resistivity of 7.1×10^{-8} $(ohm\ m)$. This brass has zero dielectric and coupling matrix properties. The brass mechanical quality factor is 1000 [34].

The piezoelectric and polymer properties can change varying the material orientation since the piezoelectric materials are transversely isotropic. This can cause a change in the harvested power. To characterize the material orientation it is used in this work the Euler angles [35] (ϕ,θ,ψ) relative to a right-handed Cartesian coordinate system. This means the material is rotated sequentially ϕ degrees around Z-axis, next θ degrees around new X-axis and finally ψ degrees around new Z-axis. The associated rotation matrix $[a]$ is presented in expressions 1 where ";" separates columns. In this work it is considered only Euler angles between -180 to 180 degrees. Each Euler angle

$$a_{1j} = [\cos\psi\cos\phi - \cos\theta\sin\phi\sin\psi\,;\cos\psi\sin\phi + \cos\theta\cos\phi\sin\psi\,;\sin\psi\sin\theta] \quad (1a)$$

$$a_{2j} = [-\sin\psi\cos\phi - \cos\theta\sin\phi\cos\psi\,;-\sin\psi\sin\phi + \cos\theta\cos\phi\cos\psi\ ;\ \cos\psi\sin\theta] \quad (1b)$$

$$a_{3j} = [\sin\theta\sin\phi\ ;-\sin\theta\cos\phi\,;\ \cos\theta] \quad (1c)$$

can assume only values going with a step of 5 degrees from -180, i. e., -180,-175,-170,-165,…,170,175,180.

2.2. Homogenization and Related FE Mesh

The method of asymptotic homogenization applied to a generic periodic microstructure made of piezoelectric materials results in macroscopic or effective or homogenized properties given by expressions 2 to 4 [13,14]. In these expressions Einstein summation convention is used and δ_{ij} is Kronecker delta. C^{EH}_{rspq} is the elasticity measured at constant electrical field, e^H_{prs} piezoelectric coupling matrix and ε^{SH}_{pq} the dielectric properties measured at constant strain. C^E_{ijkl}, e_{kij} and ε^S_{ij} are known since this are material properties. This means it is necessary to determine the characteristic displacement χ^{pq}_i, characteristic electrical potential R^p and the characteristic coupled functions Φ^p_i and Ψ^{rs} to calculate homogenized properties of the 3D periodic unit cell with domain Y. This is done using the finite element method. Details are presented in

$$C^{EH}_{rspq}(\boldsymbol{x}) = \frac{1}{|Y|}\int_Y \left[C^E_{ijkl}(\boldsymbol{x},\boldsymbol{y})\left(\delta_{ip}\delta_{jq} + \frac{\partial\chi^{pq}_i}{\partial y_j}\right) \times\left(\delta_{kr}\delta_{ls} + \frac{\partial\chi^{rs}_k}{\partial y_l}\right) + e_{kij}(\boldsymbol{x},\boldsymbol{y})\left(\delta_{ip}\delta_{jq} + \frac{\partial\chi^{pq}_i}{\partial y_j}\right)\frac{\partial\Psi^{rs}}{\partial y_k}\right]dY \quad (2)$$

$$e^H_{prs}(\boldsymbol{x}) = \frac{1}{|Y|}\int_Y \left[e_{kij}(\boldsymbol{x},\boldsymbol{y})\left(\delta_{kp} + \frac{\partial R^p}{\partial y_k}\right)\left(\delta_{ir}\delta_{js} + \frac{\partial\chi^{rs}_i}{\partial y_j}\right) - e_{kij}(\boldsymbol{x},\boldsymbol{y})\frac{\partial\Phi^p_i}{\partial y_j}\frac{\partial\Psi^{rs}}{\partial y_k}\right]dY \quad (3)$$

$$\varepsilon^{SH}_{pq}(\boldsymbol{x}) = \frac{1}{|Y|}\int_Y \left[\varepsilon^S_{ij}(\boldsymbol{x},\boldsymbol{y})\left(\delta_{ip} + \frac{\partial R^p}{\partial y_i}\right)\left(\delta_{jq} + \frac{\partial R^q}{\partial y_j}\right) - e_{kij}(\boldsymbol{x},\boldsymbol{y})\left(\delta_{kp} + \frac{\partial R^p}{\partial y_k}\right)\frac{\partial\Phi^p_i}{\partial y_i}\right]dY \quad (4)$$

with $C^{EH}_{ijkl} = C^{EH}_{klij}$; $e^H_{ijk} = e^H_{ikj}$; $\varepsilon^{SH}_{ij} = \varepsilon^{SH}_{ji}$.

[13]. The considered periodic structure finite element mesh is presented in figure 1 with the three possible forms of building a composite. This is a mesh of 14x14x14 elements. Each cube

finite element has 4 nodes. In figure 1 it can be seen a green piezoelectric material layer and an orange polymer layer. The volume fraction of piezoelectric material is given by the ratio of piezo thickness h_{piezo} and total thickness h i.e., expressions 5 and 6. The sum of piezo and polymer thicknesses is constant. This means if $v_{pz} = 1$ the microstructure is all piezoelectric material and if $v_{pz} = 0$ it is a polymer. The resultant material density is given by expression (7). The piezocomposite material damping can be estimated using a rule of mixtures [36] given by expression (8). In expressions (8) and (9) E_i is the material axial modulus of a cantilevered beam.

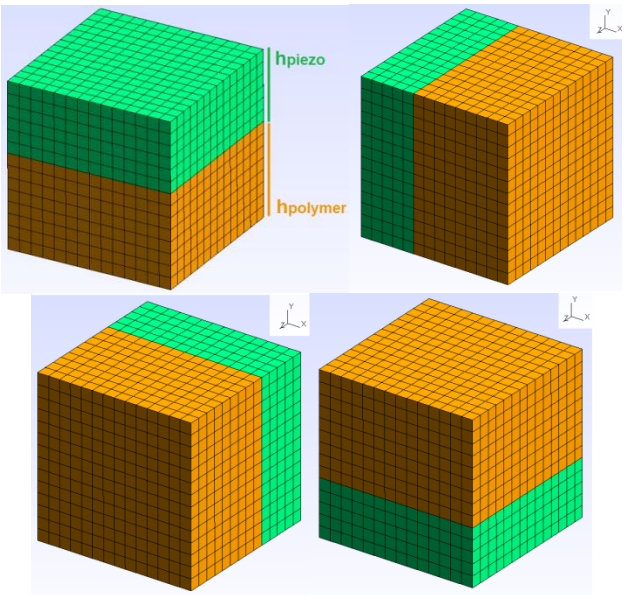

Figure 1 – Finite element mesh for periodic cell a) dimensions, b) option X, c) option Z, d) option Y

$$v_{pz} = \frac{h_{piezo}}{h} \quad (5)$$

$$h = h_{piezo} + h_{polymer} \quad (6)$$

$$\rho = \rho_{piezo} v_{pz} + \rho_{olymer}\left(1 - v_{pz}\right) \quad (7)$$

$$Q = \frac{E_{eq} Q_{piezo} Q_{polymer}}{E_{polymer}\left(1 - v_{pz}\right) Q_{piezo} + E_{piezo} v_{pz} Q_{polymer}} \quad (8)$$

$$E_{eq} = \left(1 - v_{pz}\right) E_{polymer} + v_{pz} E_{piezo} \quad (9)$$

Each cube or finite element of the piezoelectric material layer represents a single crystal or grain. If all piezoelectric material layer elements have the same orientation this means the piezoelectric material layer is a single crystal. However different orientations can be given to the different elements or crystals or grains to represent a polycrystalline piezoelectric material. In this work the crystals orientations distribution or each Euler angle distribution is assumed to follow a normal or Gaussian distribution. This means for a polycrystalline material it has to be specified each Euler angle average μ and related standard deviation σ. The probability density function is given by expression 10 where E_a is an Euler angle. With this probability density function the various orientations of the cubes or elements belonging to the piezoelectric layer are calculated.

$$p(E_a, \mu, \sigma) = \frac{1}{\sigma\sqrt{2\pi}} e^{-\left[\frac{E_a - \mu}{2\sigma^2}\right]} \quad (10)$$

3. Piezoelectric Harvesters & Harvested Power

In this work the considered piezoelectric harvester configuration is the unimorph. The configuration is presented in figure 2. In this figure it can be observed as light blue piezoelectric material and as dark blue substrate material. The yellow surfaces or surfaces referred with V_i are electrodes surfaces. A green electrical machine is connected to the electrodes. The configuration is loaded by a bending load as a harmonic tip moment. The boundary conditions presented in the figure are constrained root, i.e., a cantilevered beam. Variations of these loading and boundary conditions can be applied. The geometrical dimensions are labelled with brown color.

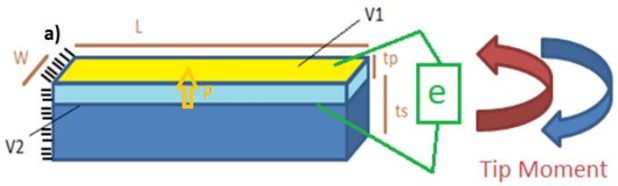

Figure 2 – Finite element mesh for periodic cell

The electrodes allow the current to flow to the electrical machine. In this work the electrical machine is a resistance (for example: a heater). The power delivered to the electrical machine is the apparent power and is given by expression 11, where R is the electrical resistance and $\bar{I}$ the complex current going into the electric machine.

$$P_a = \frac{1}{2} R |\bar{I}|^2 \quad (11)$$

4. Harvesters Finite Element Modelling

To model the unimorph harvester configuration it is used for substrate and piezoelectric materials linear piezoelectric cube elements with 20 nodes and 4 degrees of freedom (DOF): 3 translations and 1 voltage DOF. The electrodes are modelled coupling the voltage DOF for each electrode surface. To model the conductor resistivity or resistance or electrical wires it is used a 2 nodes resistance element with DOF voltage and current. It is important to note that piezoelectric materials properties inserted into the harvester simulation are the homogenized or tailored ones obtained in section 2.2.

5. Optimization Method & Design Variables

In this work what is desirable to optimize is the electrical machine harvested power, so this is the objective function:

$$O = P_a \quad (12)$$

The design variables are the Euler angles or each piezoelectric material layer orientation in the single crystal case. If the material is polycrystalline the design variables are the Euler angles and the related standard deviations for the piezoelectric layer. For the piezocomposite it is assumed a polycrystalline piezoelectric material and an orientated polymer according to three Euler angles plus the volume fraction of piezoelectric material resulting in 10 design variables for the piezoelectric layer. The Euler angles are constrained between -180 to 180 degrees assuming only discrete values as stated in section 2.1 end. The standard deviation is constrained between 0 and 5 radians going with steps of 0.1 radians.

The optimization method used is a modified simulated annealing based in the Monte Carlo step proposed in the Metropolis algorithm [14, 37]. The reason to choose a gradient free optimization method is to search relatively fast for global maximums. The algorithm is presented in annex 1 of [7]. In parallel to the algorithm it is saved the best encountered solution during the optimization. After finishing optimization the optimized and best encountered solutions are compared. It is taken the best one as the optimal. The different optimization options used in this paper are presented in table A.1 of [7].

6. Power Optimization Faraway Resonance

In this section the resistance power is optimized far away resonance, i.e., for 1 Hz loadings. In this context the mechanical quality factor can be ignored. Two loadings are considered: a tip bending moment and a tip torque.

6.1. Geometry, Loading & Boundary Conditions and Finite Element Mesh

Defined how the harvester model is created using finite elements it is necessary to specify the geometry of the different configurations. This means labelling brown variables in figure 2. The geometric values are presented in table 6.

Harvester	*L (cm)*	*W(cm)*	*tp(cm)*	*ts(cm)*
Unimorph	1	0.15	0.025	0.075

Table 6 – Unimorph dimensions

The next step is to specify the loading and boundary conditions for the two configurations thinking in terms of geometry. For the unimorph the root displacements are made equal to zero. The loading condition can be a harmonic 1 Hz tip bending moment of 0.00254 (Nm), this load case is labelled P) or a labelled T. The two loading conditions are applied as presented in figure 3 thinking about a unimorph mesh with cube elements side length 0.025 (cm), i.e., for bending a 1.2685 (N) force is applied in the four tip corners and for torque a 1.2 (N) force on each tip lateral face is applied.

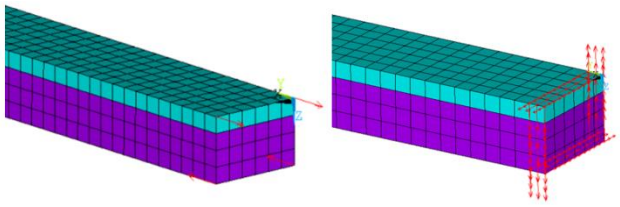

Figure 3 – Loading conditions

The unimorph mesh for converged electrical machine power results is presented in figure 4. Note in this figure referential XYZ of the piezoelectric material properties. This referential is the same as in figures 1, i.e., it gives the orientation the piezocomposite is placed on the unimorph.

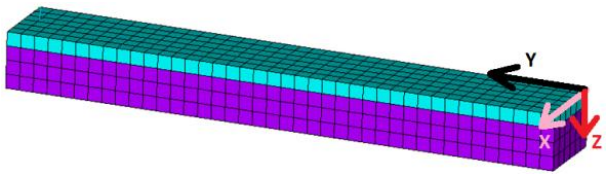

Figure 4 – Unimorph mesh

6.2. Optimization Results & Discussion

The optimization results for out of resonance scope are presented in table 7 and figure 5. In table 7 going from left column to right, it is presented the load case label, piezoelectric material, initial power output, optimization time, number of objective function evaluations, material orientation, piezoelectric material volume fraction, optimum power and power ratio. The initial power is calculated considering an initial orientation of $(\phi, \theta, \psi) = (0,0,0)$ degrees for single crystal, $(\phi_{pz}, \sigma_{\phi pz}, ; \theta_{pz}, \sigma_{\theta pz}; \psi_{pz}, \sigma_{\psi pz}) = (0, 57.3; 0, 57.3; 0, 57.3)$ degrees for polycrystalline material and for piezocomposite the same orientation as polycrystalline piezo for the piezoelectric layer, a volume fraction $v_{pz} = 0.93$ and a polymer layer orientation, $(\phi_{poly}, \theta_{poly}, \psi_{poly}) = (0,0,0)$ degrees. Looking to bending load cases power ratio, it is observed a power improvement between 2.1 and 48.5 relative to initial or classical orientation. The PZN-4.5%PT shows higher power output than the BaTio3 for the five materials options, being the ratio of maximum powers 5.50. The BaTio3 piezocomposite Pzp X material produces as much power as the polycrystalline and slightly higher power than the single crystal. This is different of what can be seen in table 7 for PZN-4.5%PT, where the optimized power for Pzp X is slightly less than polycrystalline, which is less than single crystal. For both materials the piezocomposite with the higher power output is made with 93% piezoelectric material and it is the Pzp X. Observing now the orientations associated with the bending load cases in figure 5 XXXXX. Next the unimorph is subjected to a tip torque loading, looking to the power ratio it is observed a super improvement between 580 and 43103.4. It is important to note that the initial or classical orientation extract very low power or none from the harvester. The PZN-4.5%PT continues to produce more power for the five materials options, being the ratio of maximum powers 12.5. The single crystal produces the highest power output for both PZN-4.5%PT and BaTio3 followed by the polycrystalline material. The piezocomposite which produces the highest power continues to be Pzp X. For both PZN-4.5%PT and BaTio3 the optimized piezocomposite is made with 93% piezoelectric material. Looking now associated orientations in figure 6 XXXXX. Based in these results it is concluded PZN-4.5%PT as a better material than BaTio3 for energy harvesting faraway resonance plus the optimal form of building a piezocomposite with the current materials is Pzp X. The optimization results show that having a piezocomposite with the highest possible quantity of piezoelectric material allows achieving higher power outputs. However it is important that the present optimizations don't take into account the fact that having more piezopolymer leads to an increased flexibility allowing higher deformations which can lead to higher power output. This also allows harvesting energy for situations where flexibility is required. Because we want more flexibility at the same time we want more power it is plotted in figure XXX the power vs percentage of piezoelectric material.

Load Case	Piezo Mat	P_{a_0}(pw)	Time (min)	N_{eval}	$\phi_{pz}, \sigma_{\phi pz}$ // $\theta_{pz}, \sigma_{\theta pz}$ // $\psi_{pz}, \sigma_{\psi pz}$ (deg) ϕ_{poly} // θ_{poly} // ψ_{poly} (deg)	v_{pz}	$P_{a_{max}}$ (pw)	$\frac{P_{a_{max}}}{P_{a_0}}$
B.1 Unimorph	BTO Scr	3.23e-4	56.3	253	-50 // 135 // 0	1	9.94e-3	30.8
B.2 Unimorph	BTO Pcr	8.01e-4	79.0	253	-120, 240.6 // 50, 0 // -170, 0	1	1.00e-2	12.5
B.3 Unimorph	BTO Pzp X	7.87e-4	87.7	235	-120, 240.6 // 50, 0 // -170, 0 -90 // -135 // -165	0.93	1.01e-2	12.8
B.4 Unimorph	BTO Pzp Z	0.62e-5	82.1	253	75, 131.8 // 180, 5.7 // 85, 212 80// -70 // -35	0.93	0.70e-4	11.3
B.5 Unimorph	BTO Pzp Y	2.91e-4	110.6	253	-10, 189.1 // -135, 5.7 // 140, 120.3 140 // -165 // -90	0.93	6.4e-4	2.2
B.6 Unimorph	PZN Scr	2.60e-2	75.1	253	135 // 30 // 95	1	5.55e-2	2.1
B.7 Unimorph	PZN Pcr	1.51e-3	62.6	226	-145, 143.2 // -30, 0 // -85, 5.7	1	4.31e-2	28.5
B.8 Unimorph	PZN Pzp X	1.08e-3	103.2	235	-180, 149 // 5, 0 //-60, 0 20 // -125 // 0	0.93	4.23e-2	39.2
B.9 Unimorph	PZN Pzp Z	0.27e-5	81.6	253	-35, 160.4 // 5, 5.7 // 110, 11.5 -135 // -165 // -110	0.93	0.73e-4	27.0
B.10 Unimorph	PZN Pzp Y	4.58e-4	99.9	226	-145, 143.2 // -30, 0 // -85, 5.7 -160 // 65 // -165	0.93	2.22e-2	48.5
T.1 Unimorph	BTO Scr	0	54.4	244	-70 // 125 // -45	1	2.61e-3	---
T.2 Unimorph	BTO Pcr	0.61e-6	84.1	253	150, 206.3 // 65, 0 // -50, 5.7	1	1.68e-3	2754.1
T.3 Unimorph	BTO Pzp X	0.14e-6	113.6	253	150, 206.3 // 65, 0 // -50, 5.7 30 // -55 // 45	0.93	1.75e-4	1250
T.4 Unimorph	BTO Pzp Z	0.50e-8	82.8	253	30, 286.5 // -170, 45.8 // -60, 5.7 100 // 80 // 50	0.93	0.29e-5	580
T.5 Unimorph	BTO Pzp Y	0.12e-6	112.4	253	95, 131.8 // 75, 11.5 // -145, 5.7 -30 // -45 // -55	0.93	1.24e-4	1033.3
T.6 Unimorph	PZN Scr	0	51.5	190	-135 // -135 // 45	1	3.27e-2	---
T.7 Unimorph	PZN Pcr	0.95e-6	56.7	208	-45, 166.2 // -140, 0 // -25, 0	1	1.32e-2	13894.7
T.8 Unimorph	PZN Pzp X	0.37e-6	113.9	253	-45, 166.2 // -140, 0 // -25, 0 105 // 170 // 55	0.93	6.07e-3	16405.4
T.9 Unimorph	PZN Pzp Z	0.10e-8	50.5	253	175, 108.9 // -140, 5.7 // -55, 0 -120 // -15 // 25	0.93	0.12e-4	12000
T.10 Unimorph	PZN Pzp Y	0.87e-7	73.4	253	175, 108.9 // -140, 5.7 // -55, 0 -120 // -15 // 25	0.93	3.75e-3	43103.4

Table 7 – Optimization results

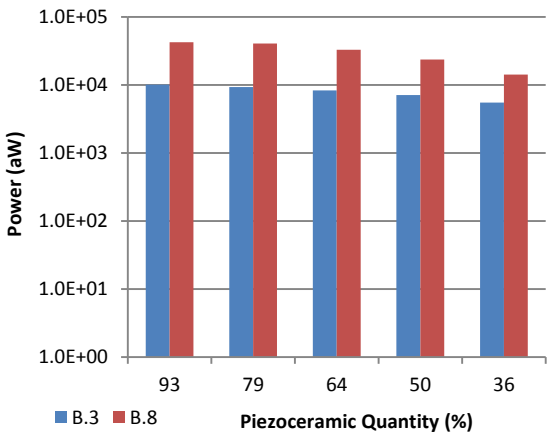

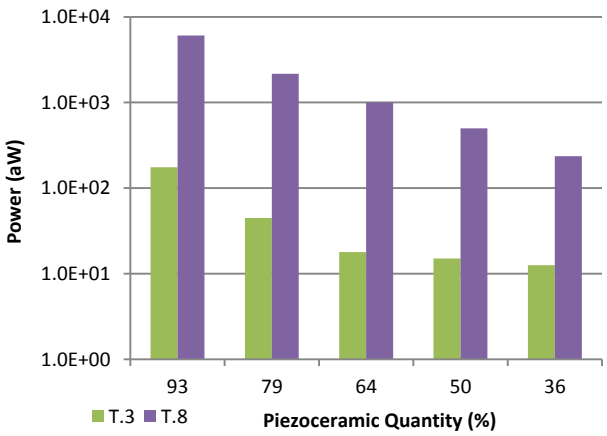

7. Power Optimization in Resonance

In this section the previous unimorph harvester is changed so that the first resonant frequency without damping and electrical power is lower than or near 140 (Hz) which is inside the range of ambient vibrations [38]. Next changed unimorph configuration power is optimized for 30 or 40 frequencies near modal frequency considering the mechanical quality factor. The mechanical quality factor measures the materials hysteretic damping and is inserted in the finite element model considering a constant damping ratio. The relation between damping ratio and mechanical quality factor is given by expression 9.

$$\zeta = \frac{1}{2Q} \quad (13)$$

7.1. Unimorph Tuning & Frequency Range

Three options are used to tune unimorph harvester first modal frequency near ambient vibrations frequencies: add a tip mass made of tantalum (a high density and high corrosion resistant material), increase beam length L_{piezo} and decrease substrate thickness S_{thick}. The tantalum properties are presented in table 8. The modified unimorph is presented in figure X. In the UniT end it is a tip mass with length $L_{tip.mass}$; this tip mass has the same width as the Unimorph of table 6.

Tantalum	*Value*
Density (Kg/m^3)	16400
Young Modulus (GPa)	186.2
Poisson Ratio	0.34

Table 8 – Tantalum mechanical properties [39]

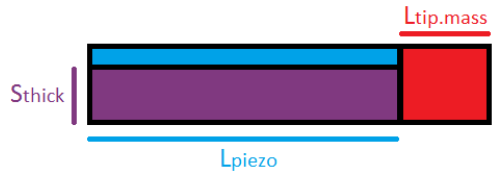

Figure 5 – UniT harvester

After studying the first modal frequency sensibility to S_{thick}, $L_{tip.mass}$ and L_{piezo} starting with Unimorph geometry with BaTio3 (0,0,0) as piezo single crystal and without electrical circuit and damping it is decided to use a UniT configuration with:

$$L_{piezo} = 5\ (cm)\ ;\ L_{tip.mass} = 0.5\ (cm)\ ;\ S_{thick} = 0.05\ (cm)$$

The first modal frequency for the different materials with (0,0,0) or classic orientation single crystal is presented in table 8.

Load Case	*Piezo Mat*	$f_1(Hz)$
B.7 UniT	BTO Scr	135.2
B.8 UniT	PZN Scr	81.3

Table 9 – 1st modal frequency

The power vs frequency for UniT is observed for the two single crystals near the modal frequencies with hysteretic damping. In this work the tantalum hysteretic damping is ignored. The resistance is considered to be 1 (ohm). It is found for BTO Scr a power peak 132.4 Hz and for PZN Scr 77.8 (Hz). With this information it is decided to do power optimization for BaTio3 in the range 120 to 150 Hz and for PZN in the range 65 to 105 Hz.

7.2. Objective Function and Optimization Results

Near resonance the objective function needs to be changed since it is desired to capture the power curve behavior near the peak. To do this the objective function is changed to expression 10. This expression is the power sum over N different frequencies. In this work $N = 30$ and since the power range is 30 Hz for both BaTio3 and PZN this means power will go up with a 1Hz step starting on 120 for BTO and 65 for PZN.

$$O = \sum_{i=1}^{N} P_{a_i} \quad (14)$$

The optimizations are run for common piezoelectric material and polycrystalline materials. Piezocomposites are not considered since it is not yet developed a method to calculate material homogenized mechanical quality factor. The results are presented in table X and figures Y.

Load Case & Configuration	*Piezo Mat*	P_{a_0}*(pw)*	*Time (min)*	N_{eval}	$\phi_{pz}, \sigma_{\phi pz}$ // $\theta_{pz}, \sigma_{\theta pz}$ // $\psi_{pz}, \sigma_{\psi pz}$ (deg) ϕ_{poly} // θ_{poly} // ψ_{poly} (deg)	v_p	$P_{a_{max}}$ *(pw)*	$\frac{P_{a_{max}}}{P_{a_0}}$
B.7 UniT	BTO Scr	XXX	615.4		-40 // -55 // -175	1	3026.3	
B.8 UniT	BTO Pcr					1		
B.9 UniT	BTO Pzp							
B.10 UniT	PZN Scr					1		
B.11 UniT	PZN Pcr					1		
B.12 UniT	PZN Pzp							

References

[1] H. A. Sodano, D. J. Inman & G. Park. *A review of power harvesting from vibration using piezoelectric materials*. Shock and Vibration Digest, volume 36, pages 197-206. 2004

[2] S. R. Anton & H. A. Sodano. *A review of power harvesting using piezoelectric materials (2003-2006)*. Smart Materials and Structures, volume 16, number 3. 2007

[3] L. Zhang, K. A. Williams & Z. Xie. *Evaluation of Analytical and Finite Element Modeling on Piezoelectric Cantilever Bimorph Energy Harvester*. Transactions of the Canadian Society for Mechanical Engineering, Volume 37, Number 3. 2013

[4] V. Piefort. *Finite Element Modelling of Piezoelectric Active Structures*. PhD Thesis, Université Libre de Bruxelles, Belgium. 2001

[5] C. M. Junior, A. Erturk, D. J. Inman. *An electromechanical finite element model for piezoelectric energy harvester plates*. Journal of Sound and Vibration, volume 327, pages 9-25. 2009

[6] J. B. Min, K. P. Duffy, B. B. Choi, A. J. Provenza & N. Kray. *Piezoelectric Vibration Damping Study for Rotating Composite Fan Blades*. NASA/TM-2012-217648, USA. 2012

[7] A.M. Matos, J.M. Guedes, K.P. Jayachandran, H.C. Rodrigues. *Piezoelectric Vibrations Energy Harvesters Power Optimization Using the Finite Element Method*. In house work

[8] W. Smith, A. Shaulov & B.A. Auld. *Tailoring the Properties of Composite Piezoelectric Materials for Medical Ultrasonic Transducers*. IEEE Ultrasonics Symposium. 1985

[9] K. Uchino. Ferroelectric Devices. Material Engineering, CRC Press. 2000

[10] X.Y. Zhou, H.S. Gu, Y. Wang & T.S. Zhou. *Piezoelectric properties of Mn-doped* $(Na_{0.5}Bi_{0.5})_{0.92}Ba_{0.08}TiO_3$ *ceramics.* Materials Letters, volume 59, pages 1649-1652. 2005

[11] R. Zuo, C. Ye, X. Fang & J. Li. *Tantalum doped* $0.94Bi_{0.5}Na_{0.5}TiO_3$–$0.06BaTiO_3$ *piezoelectric ceramics.* Journal of the European Ceramic Society, volume 28, pages 871-877. 2007

[12] P. W. Rehrig et al. *Piezoelectric properties of zirconium-doped barium titanate single crystals grown by templated grain growth*. Journal of Applied Physics, volume 86, pages 1657-1661. 1999

[13] E.C.N. Silva, J.S.O. Fonseca & N. Kikuchi. *Optimal design of periodic piezocomposites*. Computer Methods in Applied Mechanics and Engineering, volume 159, pages 49-77. 1998

[14] K. P. Jayachandran, J. M. Guedes & H. C. Rodrigues. *Optimal configuration of microstructure in ferroelectric materials by stochastic optimization*. Journal of Applied Physics, volume 108, issue 2. 2010

[15] K. P. Jayachandran, J. M. Guedes & H. C. Rodrigues. *Piezoelectricity enhancement in ferroelectric ceramics due to orientation.* Applied Physics Letters, volume 92, issue 23. 2008

[16] J. M. Guedes & N. Kikuchi. *Preprocessing and Postprocessing for Materials Based on the Homogenization method with Adaptive Finite Element Methods*. Computer Methods in Applied Mechanics and Engineering, volume 83, pages 143-198. 1990

[17] P.G. Coelho, S.J. Hollister, C.L. Flanagan & P.R. Fernandes. *Bioresorbable scaffolds for bone tissue engineering: optimal design, fabrication, mechanical testing and scale-size effects analysis*. Medical Engineering and Physics. Already published. 2014/2015

[18] M. Syha et al. Three-dimensional grain structure of sintered bulk strontium titanate from X-ray diffraction contrast tomography. Scripta Materialia, volume 66, pages 1-4. 2012.

[19] P. Reischig et al. *Advances in X-ray diffraction contrast tomography: flexibility in the setup geometry and application to multiphase materials*. Journal of Applied Crystallography, volume 46, pages 297-311. 2013

[20] T.L. Jordan, Z. Ounaies. *Piezoelectric Ceramics Characterization*. NASA/CR-2001-211225, USA. 2001

[21] P. Zheng, J.L. Zhang, Y.Q. Tan & C.L. Wang. *Grain-size effects on dielectric and piezoelectric properties of poled* $BaTiO_3$ *ceramics*. Acta Materialia, volume 60, pages 5022-5030. 2012

[22] M. Zgonik et al. *Dielectric, elastic, piezoelectric, electro-optic, and elasto-optic tensors of BaTiO3 crystals*. Physical Review B, volume 50, pages 5941-5949. 1994

[23] J. Yin, B. Jiang & W. Cao. *Elastic, Piezoelectric, and Dielectric Properties of* $0.955Pb(Zn_{1/3}Nb_{2/3})O_3$-$0.45PbTiO_3$ *Single Crystal with Designed Multidomains*. IEEE Transactions on Ultrasonics Ferroelectrics and Frequency Control, volume 47, pages 285-291. 2000

[24] W. Shu, J. Wang & T. Zhang. *Effect of grain boundary on the electromechanical response of ferroelectric polycrystals*. Journal of Applied Physics, volume 112, issue 6. 2012

[25] H. S. Kim, J. H. Kim, J. Kim. *A Review of Piezoelectric Energy Harvesting Based on Vibration*. International Journal of Precision Engineering and Manufacturing, volume 12, pages 1129-1141. 2011

[26] D. J. Li et al. Polymer piezoelectric energy harvesters for low wind speed.

[27] D. A. Ende, H. J. Wiel, W. A. Groen & S. Zwaag. *Direct strain energy harvesting in automobile tires using piezoelectric PZT-polymer composites*. Smart Materials and Structures, volume 21, number 1. 2012

[28] R. Kar-Gupta & T.A. Venkatesh. *Electromechanical response of 1-3 piezoelectric composites: An analytical model*. Acta Materialia, volume 55, pages 1093-1108. 2007

[29] D. Kobor et al. Mn *Effect on Nonlinear and Structural Properties of <110> Oriented PZN-4.5PT Single Crystals*. Journal of Modern Physics, volume 3, pages 404-411. 2012

[30] Internet Website APC International, Properties of BaTio3 https://www.americanpiezo.com/product-service/bati03.html. 12/11/2014

[31] Van Son Nguyen et al. Flexible *Over-Moded Resonators Based on P(VDF-TrFE) Thin Films With Very High Temperature Coefficient*. IEEE Transactions on Ultrasonics, Ferroelectrics, and Frequency Contro, Volume 60, pages 2039-2043. 2013.

[32] Internet Website E-ZLOK, Technical Info, Free-Cutting Brass. http://www.ezlok.com/TechnicalInfo/MPBrass.html . 04/11/2014

[33] Internet Website The Engineering ToolBox, Resistivity. http://www.engineeringtoolbox.com/resistivity-conductivity-d_418.html . 04/11/2014

[34] K. Nakamura, K. Kakihara, M. Kawakami & S. Ueha. *Measuring vibration characteristics at large amplitude region of materials for high power ultrasonic vibration system*. Ultrasonics, volume 38, pages 122-126. 2000

[35] H. Goldstein. *Classical Mechanics*. Addison-Wesley. 1978

[36] D.A. Saravanos and C.C. Chamis. *Unified ;Micromechanics of Damping for Unidirectional Fiber Reinforced Composites*. NASA Technical Memorandum 102107. 1989

[37] J. S. Arora. *Introduction to Optimum Design*. Elsevier Academic Press. 2004

[38] S. Roundy, P.K. Wright & J. Rabaey. *A study of low level vibrations as a power source for wireless sensor nodes*. Computer Communications, volume 26, pages 1131-1144. 2003

[39] Internet Website Efunda, Materials Data, Elements. http://www.efunda.com/materials/elements/element_info.cfm?Element_ID=Ta . 07/11/2014